J. Quant. Spectrosc. Radiat. Transfer Vol. 49, No. 5, pp. 467–483, 1993
Printed in Great Britain. All rights reserved

0022-4073/93 $6.00 + 0.00
Copyright © 1993 Pergamon Press Ltd

OPTICALLY THIN CIRRUS CLOUDS: RADIATIVE IMPACT ON THE WARM POOL

C. PRABHAKARA,† D. P. KRATZ,‡ J.-M. YOO,§ G. DALU,¶ and A. VERNEKAR||

†Laboratory for Atmospheres, NASA/GSFC Greenbelt, MD 20771, ‡Lockheed Engineering & Sciences Co., Hampton, VA 23666, §Applied Research Corp., Landover, MD 20785, U.S.A. ¶C.N.R., Istituto di Fisica dell' Atmosfera, Rome, Italy and ||Department of Meteorology, University of Maryland, College Park, MD 20742, U.S.A.

(Received 6 August 1992)

Abstract—Over the convectively active tropical ocean regions, measurements made from space in the infrared (i.r.) and visible have revealed the presence of optically thin cirrus clouds which are quite transparent in the visible and nearly opaque in the infrared. The *Nimbus 4* Infrared Interferometer Spectrometer (IRIS), which has a field of view (FOV) of ≈ 100 km, has been utilized to examine the i.r. optical characteristics of these cirrus clouds. From the IRIS data it has been observed that these optically thin cirrus clouds prevail extensively over the "warm pool" region of the equatorial western Pacific surrounding Indonesia. It is found that the seasonal cloud cover produced by these thin cirrus exceeds 50% near the central regions of the "warm pool". For most of these clouds, optical thickness in the infrared is <2. It is deduced that dense cold anvil clouds associated with deep convection spread extensively and are responsible for the formation of the thin cirrus. This is supported by the observation that the coverage of the dense anvil clouds is an order of magnitude less than that of the thin cirrus. Observations made by the Earth Radiation Budget Experiment (ERBE) reveal that the "warm pool" region constitutes a local maximum in net input of radiative energy. From these observations, together with a simple radiative energy balance model, we have inferred that the greenhouse effect produced by the optically thin cirrus clouds can be a significant factor in maintaining the "warm pool".

1. INTRODUCTION

The "warm pool" area, located in the equatorial western Pacific, has sea-surface temperatures that exceed 28°C in all seasons. As revealed by satellite measurements, the "warm pool" region is usually cloud-covered and is characterized by low values of the outgoing longwave radiation (OLR), ≈ 200 W/m^2.[1] Moreover, the investigation of Barkstrom et al[2] has shown that the "warm pool" is a region of local maximum in net radiation (the solar incoming minus OLR) at the top of the atmosphere. This maximum in net radiation is ~ 80 W/m^2. Another remarkable aspect of this region is that there is on the average about 10 mm/day of rain.[3] By combining this salient information, together with a knowledge of the transports prevailing in the atmosphere and the ocean, up to a depth of the thermocline, it is possible to explain how the elevated temperatures in the "warm pool" are maintained. The errors in the estimation of the various energy processes at present, however, are such that it is difficult to draw definitive conclusions. To resolve this situation, the TOGA–COARE (World Climate Research Program) program[4] will make extensive measurements to help improve our understanding of the energy budget.

The purpose of the present study is to discuss the role of the radiative effects of thin cirrus clouds in the energy balance of the "warm pool" region. The available evidence indicates that the impact of the thin cirrus clouds is to radiatively produce a local heat source, which appears to be a significant factor in maintaining the "warm pool".

Several studies[5–7] have discussed the role of clouds in the atmosphere as regulators of the radiative energy balance. From observations, it has been deduced that clouds found primarily at low altitudes, such as stratiform clouds in the boundary layer, lead to a net cooling, since they reflect a significant percentage of the incoming solar energy while radiating to space in the infrared (i.r.) at fairly warm temperatures.[8]

The high altitude cirrus and cirrostratus clouds, however, radiate to space in the i.r. at a much cooler temperature which can result in a net warming. In the context of the global warming caused

by increase in CO_2 and other trace gases, the role of the clouds in the atmosphere must be understood and properly taken into consideration.

Satellite observations in the i.r. and visible[9–12] have revealed some of the interesting properties of the cold high altitude cirrus clouds that prevail over the "warm pool". Other studies[7,13] have also discussed the nature of the optically thin cirrus clouds. Platt et al[13] suggest that in the cold upper tropospheric regions, where there are small amounts of water vapor, the optically thin cirrus clouds present tend to be fairly transparent to incoming solar radiation while being nearly opaque to the outgoing i.r. These optical properties of the thin cirrus clouds have the potential to lead to a greenhouse warming. To date, the extent to which such a greenhouse warming is affecting the Earth has not been assessed because of the lack of data concerned with the geographic extent of the thin cirrus and their i.r. optical depth. Based on a recent study,[10] it is now possible to derive the necessary information from the data obtained by the Infrared Interferometer Spectrometer (IRIS) that was flown on the *Nimbus 4* satellite in 1970.

A brief account of the IRIS and a method to estimate the thin cirrus information is presented in Sec. 2. A simple radiative energy balance model that is applicable to the mesoscale convective systems in the "warm pool" is developed in Sec. 3. This radiative energy balance model, which does not explicitly take into account the transports, is used to demonstrate the net radiative heating produced by the thin cirrus clouds.

2. SATELLITE OBSERVATIONS ON THIN CIRRUS

The IRIS on board *Nimbus 4* provided valuable data for about 10 months: April 1970–January 1971. This spectrometer viewed the Earth at nadir with a field of view of about 100 km and had a spectral resolution of 2.8 cm^{-1} in the i.r. region, 7–25 μm (see Hanel et al,[9] for more details on IRIS). In a study based on these high resolution IRIS data, Prabhakara et al[10] inferred the presence of optically thin cirrus clouds over the convective areas of the oceans namely the "warm pool" region, the Intertropical Convergence Zone (ITCZ) and the South Pacific Convergence Zone (SPCZ).

From the IRIS observations, it is deduced that the thin cirrus clouds have a spatial scale of about a few hundred kilometers. Based on these observations, one can also infer that these thin cirrus clouds result from the spreading of the thick anvil clouds that have cold tops of ≈ 220 K. The scale of these complex cloud structures suggests that they are associated with mesoscale convective systems (MCS) that prevail in the convective areas.

In Fig. 1, a schematic picture of the MCS over the "warm pool" area is shown with a mature cumulonimbus anvil and some cumulus clouds at low altitude in different stages of development. Under the outer reaches of the anvil there can be open ocean with no cumulus underneath. The IRIS spectra are well suited to distinguish the character of the cirrus clouds in the MCS. To demonstrate this point, a clear sky spectrum over the oceans and a spectrum of an oceanic scene containing an optically thin cirrus[10] over the ocean are displayed in Figs. 2 (a and b), respectively.

Unlike molecular absorption, which exhibits fine spectral structure, clouds tend to produce broad spectral features. A very prominent cloud extinction feature stretches from 980 to 750 cm^{-1} (10.2–12.9 μm). This cloud extinction feature produces an enhanced difference between the brightness temperatures at 11 and 13 μm (910 and 770 cm^{-1}), and can be readily identified (Fig. 2b) by its effect upon the window region spectrum between the 9.6 μm O_3 band and the 15 μm CO_2 band. In addition, cloud extinction inferred from the IRIS spectra for the spectral region from 550 to 400 cm^{-1} (from 18 to 25 μm), where the water vapor rotation band is present, reinforces the conclusions drawn from the observations made in the window region.

Because of the presence of water vapor in the Earth's atmosphere, especially in the first few kilometers above the sea surface, the brightness temperature in the window region decreases from 980 to 775 cm^{-1} for clear sky conditions. This decrease in the brightness temperature from 11 to 13 μm, $\Delta T = T_{11} - T_{13}$, can be as large as 5°C in the humid "warm pool" region. Under these conditions, the value of T_{11} is about 293 K; however when there is an optically thin cirrus on the scene, ΔT is significantly greater than 5°C and T_{11} is several degrees below 293 K. The brightness temperature in the rotation band region at 18 μm, T_{18}, is also reduced by thin cirrus. As shown in Prabhakara et al,[10] the ΔT in the optically thin cloud cases can be related to the cloud properties

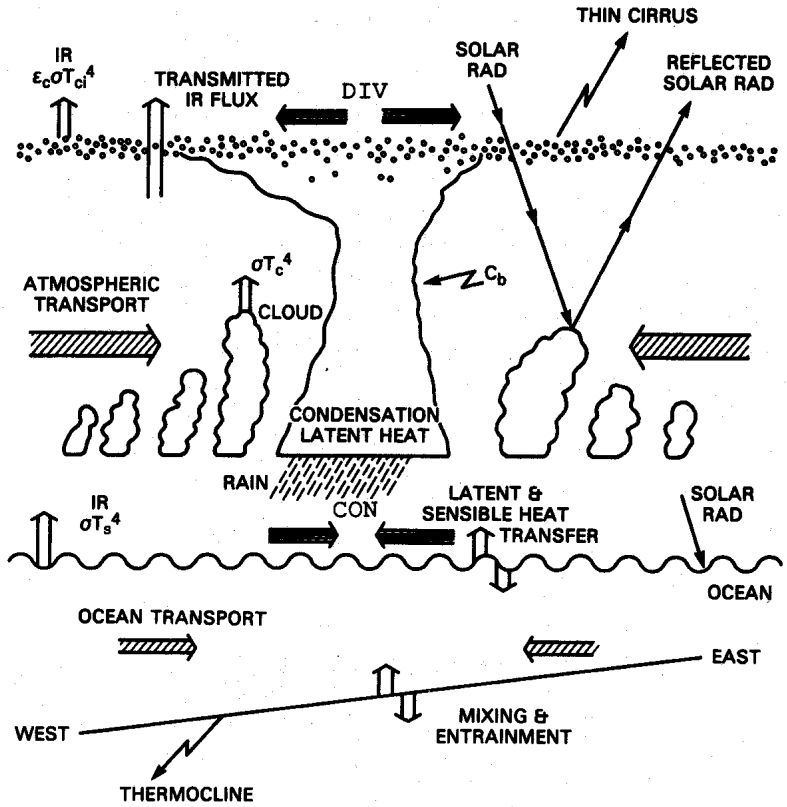

Fig. 1. Schematic figure of the mesoscale convective system containing optically thin cirrus produced by spreading of deep convective cumulonimbus anvil. Depicted in the figure are (a) weak cumulus underlying the cirrus, (b) radiative processes at the sea surface and within the atmosphere, including cumulus and thin cirrus, and (c) energy transports in the atmosphere and the ocean.

with the help of the radiative transfer theoretical calculations that take into account the absorption and scattering by the cirrus ice particles. Unlike the optically thin cloud, whose absorption is wavelength dependent, the optically thick cloud emits like a blackbody and, hence, ΔT is small. If we assume this optically thick cloud top is around 11 km, the brightness temperature at 11 μm is some 70 K below the SST.

The discussion of the cloud spectra presented above is applied to a large MCS complex observed over the "warm pool" around local noon on 16 October 1970. In order to understand this case,

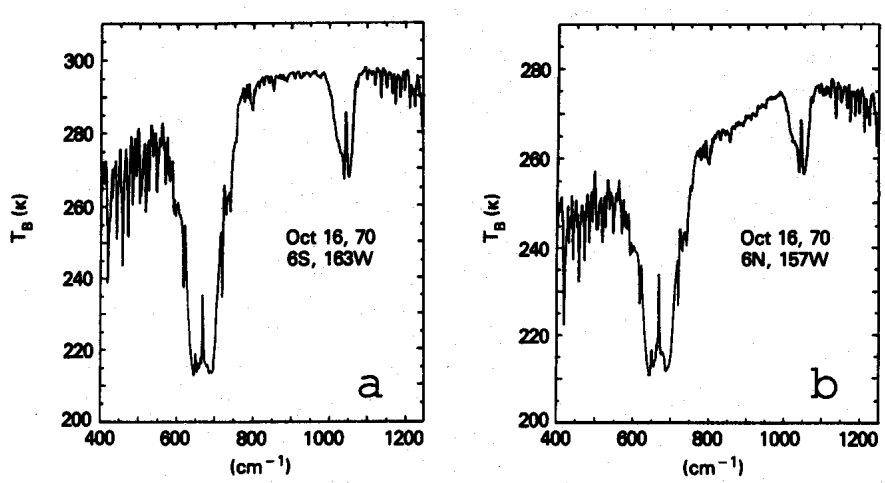

Fig. 2. IRIS spectra observed over the tropical oceans. (a) Cloud-free tropical ocean spectrum, and (b) Maritime tropical spectrum contaminated by optically thin cirrus.

12 spectra observed by IRIS along one orbital track as the satellite passed northward from about 4°S and 167°E to 7°N and 164°E, are presented in Fig. 3. Each of these spectra show some degree of cirrus cloud contamination with the exception of spectrum 7 near 0.3°N, which has the largest values of T_{11} and T_{18} (292 and 267 K, respectively), and the smallest value of ΔT (5.6 K). It is straightforward to see that the spectra 3 and 4, where the 15 μm CO_2 and the 9.6 μm O_3 bands are weak and $T_{11} \approx 225$ K, correspond to high cold clouds in the center of the MCS complex. The spectra on either side of the MCS center, i.e. 1 and 2, and 5 and 6 show a gradual warming and suggest a decrease in the effect of the dense clouds and an increase in the effect of the optically thin clouds. This is evident from the values of T_{11}, ΔT, and T_{18} identified in these spectra.

Spectra 8, 9, 10, 11, and 12 are influenced by some MCS that are outside the subsatellite track of the IRIS observations. The presence of the thin cirrus background in these spectra can be deduced, however, from their spectral characteristics (i.e. T_{11}, ΔT, and T_{18}). This can be appreciated

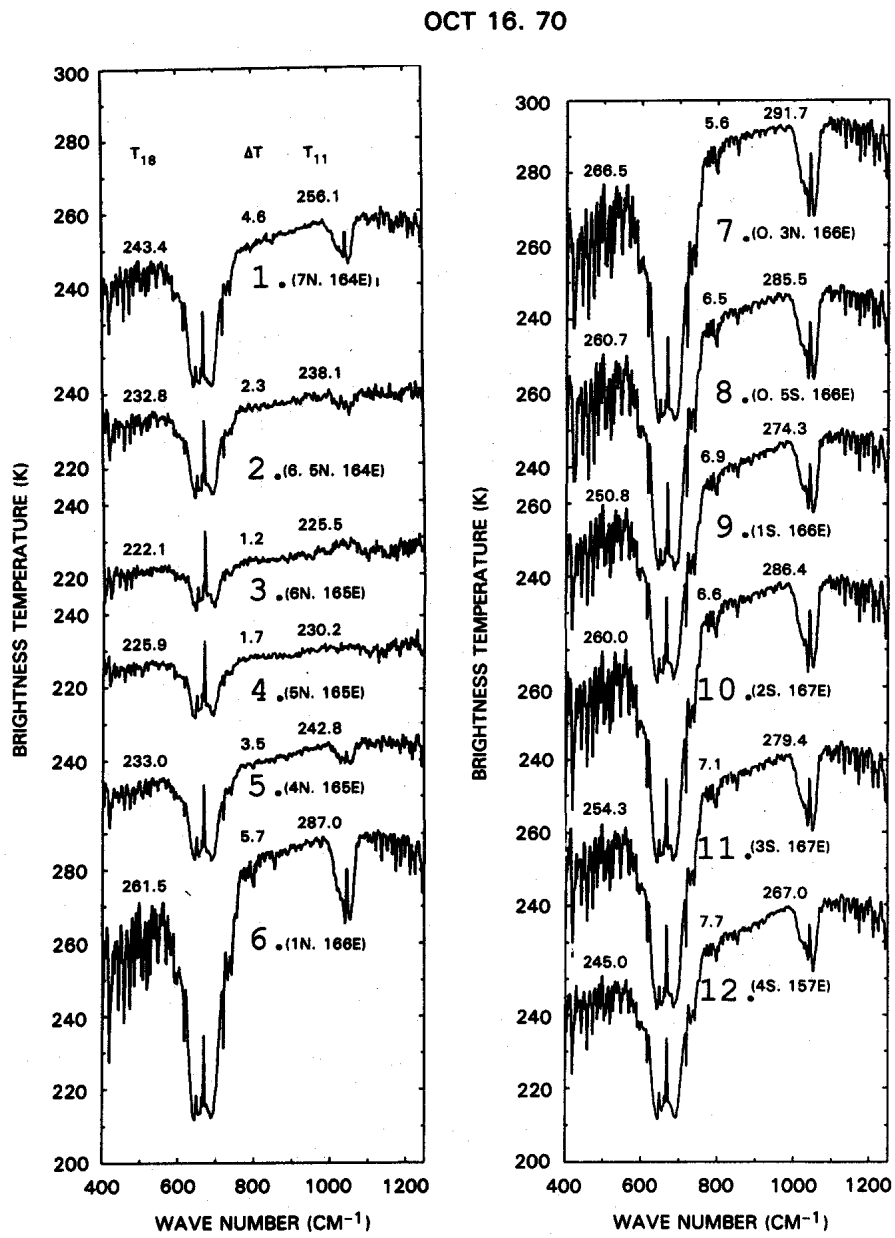

Fig. 3. IRIS spectra observed along one orbital track as the satellite passed northward from about 4°S, 167°E to 7°N, 164°E on 16 October 1970. The spectra are numbered 1–12, starting with 7°N as 1 and ending with 4°S as 12. Each spectrum is identified with its location and spectral details pertaining to $T_{10.8}$, ΔT and T_{18}. The spectra are compacted along the ordinate with separate ordinate values.

by contrasting these spectra with that of spectrum 7. All of these cloud spectra give an indication of the massive aerial extent of thin cirrus over the "warm pool".

In the theoretical calculation, Prabhakara et al[10] assumed the cirrus ice particles are spherical, having a log normal size distribution with an effective radius, r_e. The value of brightness temperature calculated from this theoretical model for the relatively narrow spectral intervals at 11 and 13 μm is shown to have the following functional dependence:

$$T_{11} = f\,[(T_s - T_c), m, k_{11}(r_e), \omega_{11}(r_e)]$$
$$T_{13} = f\,[(T_s - T_c), m, k_{13}(r_e), \omega_{13}(r_e)] \qquad (1)$$

where T_s is the sea surface temperature, T_c is the temperature of the cirrus cloud layer, which is assumed to be isothermal; m(g/cm^2) is the mass of the ice particles in a column of the cloud; k_{11} and k_{13} (cm^2/g) are the extinction cross sections of the ice particles in the cloud whose effective radius is r_e; and ω_{11} and ω_{13} are the corresponding single scattering albedo values. It follows from Eq. (1) that for a given $(T_s - T_c)$ and r_e, T_{11} and T_{13} are dependent on m, the mass of the particles in a vertical column of the cloud. Hence the difference $\Delta T = T_{11} - T_{13}$ is also a function of m. Results of theoretical calculations[10] are illustrated in Fig. 4 for a family of cirrus clouds with particle sizes r_e ranging between 1.5 and 24 μm and the total extinction optical depth, τ_{11}, ranging from 0 to 20. Underneath the cirrus, it is assumed there are no other clouds, and the surface temperature, T_s, is 301 K, while the temperature of the cirrus clouds, T_c, is taken to be 230 K. In Fig. 4, ΔT is plotted as a function of the brightness temperature T_{11} since both these quantities are measurable. It can be observed that the curves of ΔT vs T_{11} for different values of r_e have a maximum ΔT in the vicinity of $T_{11} \approx 270$ K. This maximum is quite pronounced for small ice particles whose $r_e \leqslant 6\,\mu$m. The isolines of optical depth τ_{11} are shown in the Fig. 4. These isolines reveal that ΔT maximum is close to $\tau_{11} = 1$. An important result obtained from these theoretical calculations is that the extinction caused by the thin cirrus clouds is mainly responsible for decreasing T_{11} below 290 K and increasing ΔT above 5 K. Water vapor absorption alone cannot explain such results.

In Fig. 5 the IRIS observations over the tropical ocean (10°S to 10°N) are plotted as a function of ΔT vs T_{11} to illustrate the correspondence between theory and observations.

In Fig. 6 the theoretical frame work developed above is applied to the IRIS data over the equatorial Pacific. Here the IRIS observations, made during 3 months at four oceanic regions of 10° lat × 10° long size, are presented in the form of frequency distribution in the space defined by

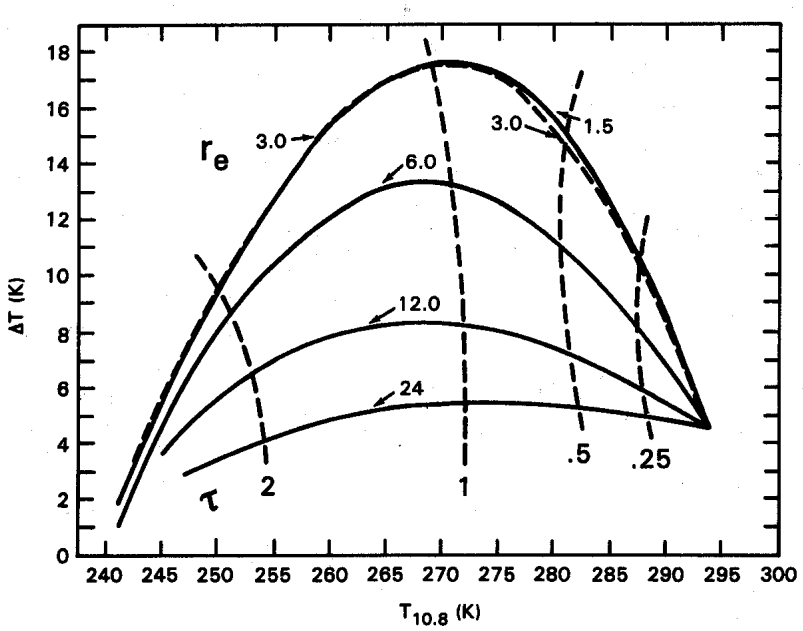

Fig. 4. Theoretical values of ΔT vs $T_{10.8}$ for high-level (cirrus) spherical ice crystal clouds as a function of particle size and optical depth. The solid isolines of particle size r_e and dashed isolines of optical depth, τ are identified. (Note: isoline of $r_e = 3\,\mu$m is also dashed.)

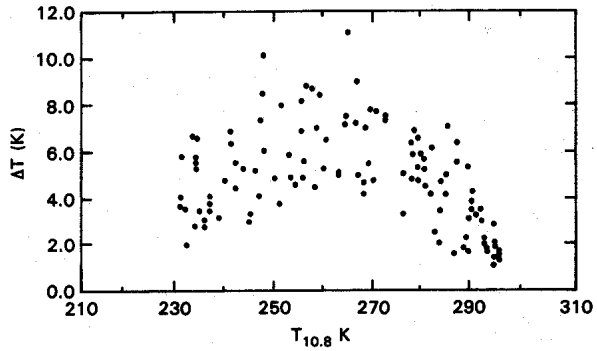

Fig. 5. The temperature difference, ΔT vs $T_{10.8}$ derived from the IRIS data over the tropical oceans (10°N–10°S).

the two variables ΔT and T_{11}. Two of these oceanic regions represent the "warm pool" during the northern summer and fall seasons. The other two regions are chosen to reveal the character of the dry tropical eastern Pacific, where the subsidence in the atmosphere and the oceanic upwelling are dominant. The IRIS data over the "warm pool", Figs. 6 (a and b), when compared with the theoretical results, Fig. 4, show some gross similarities. It should be noted that in observations involving diverse natural situations, other clouds such as cumulus (see Fig. 1) may be present between the sea surface and cirrus, which can introduce a significant spread in the data presented in Figs. 6 (a and b). Thus, one has to take into consideration these variable conditions when comparing the theoretical results with the IRIS data. Despite these limitations, one observes that the ΔT maximum in both the figures is close to $T_{11} \approx 270$ K. The magnitude of ΔT maximum of about 10 K in the data, when compared with that in Fig. 4, suggests that r_e for such clouds is about 6 μm.

The percentage cloud cover caused by thin cirrus and their optical depth can be estimated with the help of the analysis presented above. Based on the arguments presented earlier, if we assume the IRIS data shown in Figs. 6 (a and c) (where $T_{11} < 290$ K and $\Delta T > 5$ K) represent thin cirrus in the whole field of view, then we can get an estimate of their percentage. Such estimates over the "warm pool" region are shown to reach $\approx 60\%$. On the contrary, over the dry subsidence regions, Figs. 6 (b and d), the cirrus amount is negligibly small. Another important observation is that in the "warm pool" events the high cold clouds, $T_{11} < 225$ K, constitute only a small fraction $\approx 5\%$ of the total number of cases. These high cold clouds are optically dense cirrus.

We may note that over the convectively active region we do not expect the presence of large scale subsidence. Hence, the extensive stratiform clouds that are generally underneath the subsidence inversion are not present here. This leaves us with primarily two possible cloud configurations over the "warm pool". One in which there is clear ocean with some fair weather shallow cumulus clouds. This happens when there is a lull in the convection. On the other hand when convection is taking place the MCS's are present as described earlier in Fig. 1. This picture of the cloud system will be helpful in the assessment of the radiation energy balance that is presented in the next section.

Using this technique, the percentage of optically thin cirrus over the tropical oceans from 25°N to 25°S is deduced from IRIS measurements for four seasons as shown in Figs. 7–10. In order to illustrate the significance of the inferred thin cirrus, the climatology of sea surface temperature (SST) is shown in Figs. 11 and 12 for two seasons. The striking similarity between the distribution of thin cirrus clouds and the SST over the tropical oceans, and in particular over the "warm pool" region, is clearly revealed. Note that the maxima of these two variables move poleward during the local summer season.

A weighted mean optical depth of these thin cirrus clouds can be assessed as follows. If one takes the population of clouds with $T_{11} < 290$ K and $\Delta T > 5$ K, it is found that the weighted mean $\bar{\tau}_{11}$ of such population is approx 1.0 ($\bar{\tau}_{11} = \Sigma \tau_i f_i / \Sigma f_i$, where f_i is the frequency of observations, also note from Figs. 4 and 6 that this population of cirrus clouds has $2 > \tau_{11} > 0$).

3. SIMPLE RADIATIVE ENERGY BALANCE MODEL

Optically thin cirrus clouds, which are more transparent in the visible than in the i.r. are produced by MCS. They are present over a substantial area of the "warm pool" and therefore should have

important implications to the local energy balance. The energetics of the "warm pool" are not fully understood (see World Climate Research Program[4] for an extensive discussion and list of references) and the role played by cirrus clouds is poorly appreciated.

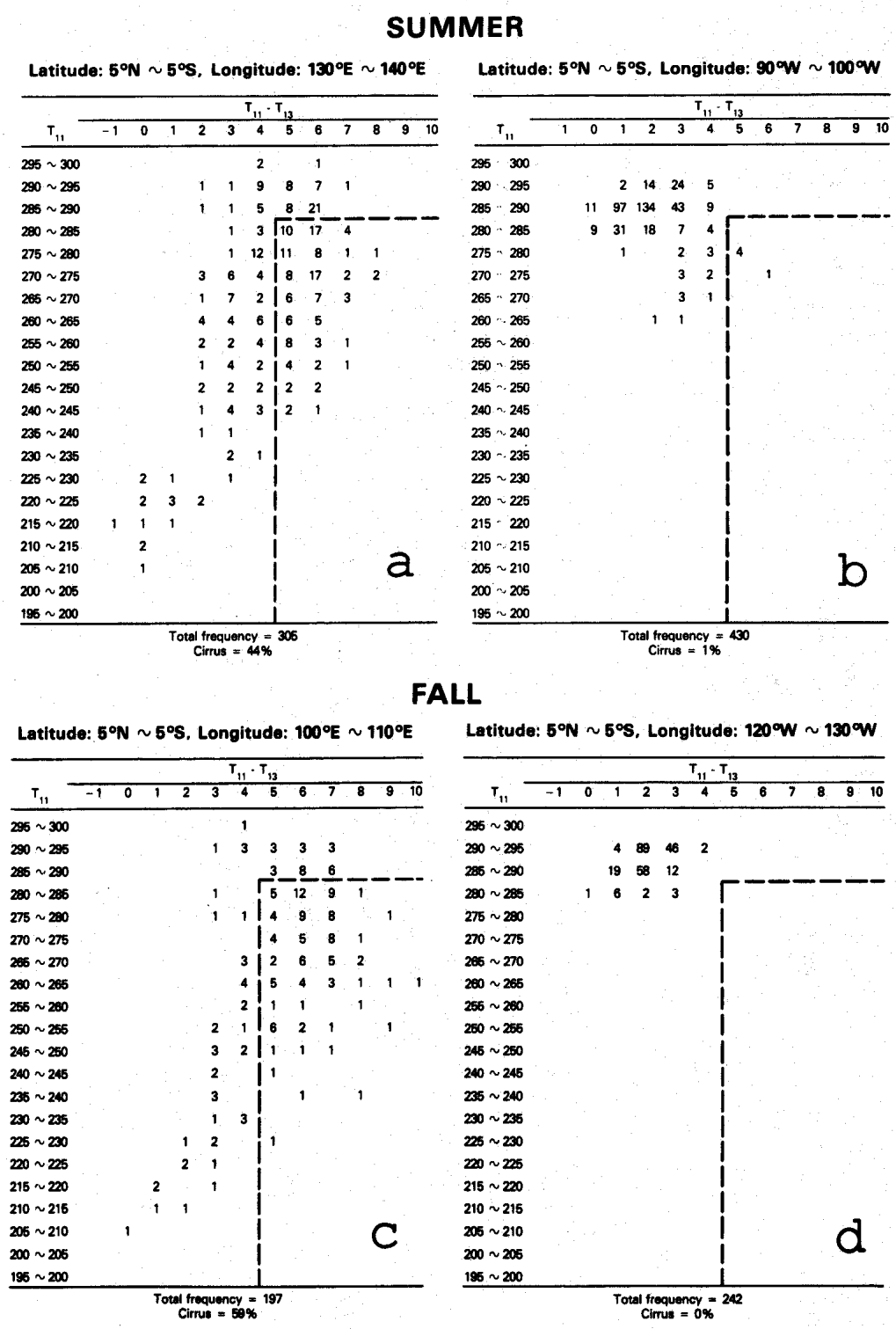

Fig. 6. Frequency distributions of seasonal IRIS data as a function of ΔT and $T_{10.8}$ over the 10° lat × 10° long oceanic regions for different seasons. Dashed vertical and horizontal lines delineate the thresholds on ΔT and $T_{10.8}$. Both total frequency and cirrus percentage as also shown. (a) June, July, and August (5°N–5°S, 130°E–140°E), (b) June, July, and August (5°N–5°S, 90°W–100°W), (c) September, October, and November (5°N–5°S, 100°E–110°E), and (d) September, October, and November (5°N–5°S, 120°W–130°W).

First, let us note in a brief manner the dynamical processes that prevail in the ocean and atmosphere over the "warm pool". In the absence of an El Nino event this region functions as a system that is statistically in a dynamic equilibrium. This is reflected by the coupling between the short-lived MCS events that produce precipitation, and the large scale circulation that leads to convergence of moisture. The surface wind stress, that produces up-welling and a shallow thermocline on the eastern equatorial Pacific, leads to a containment of the warm waters with a deep thermocline on the western equatorial Pacific. This wind stress essentially inhibits rapid mixing of warm water on the west with the cooler water to the east.

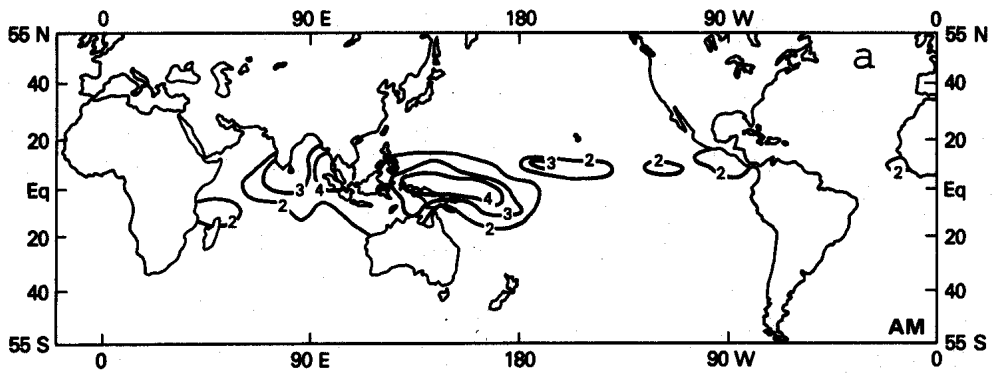

Fig. 7. Seasonal percentage cloud cover caused by optically thin cirrus in the tropics between 25°N and 25°S during April and May. The numbers should be multiplied by 10 to get percent cloud cover.

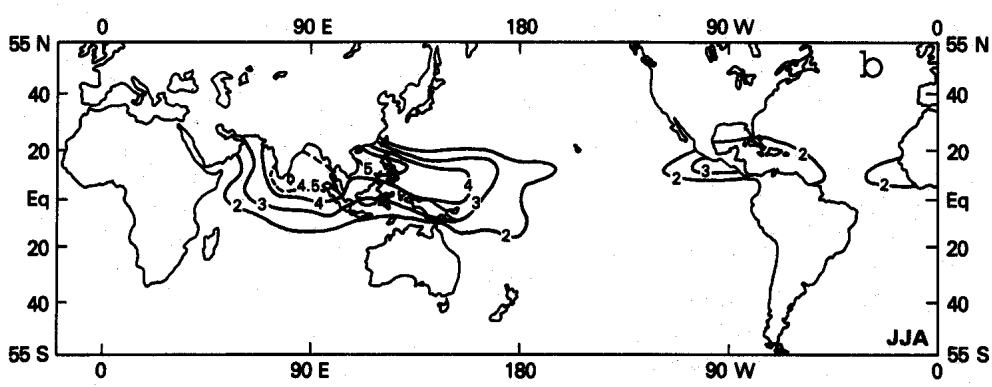

Fig. 8. Seasonal percentage cloud cover caused by optically thin cirrus in the tropics between 25°N and 25°S during June, July, and August. The numbers should be multiplied by 10 to get percent cloud cover.

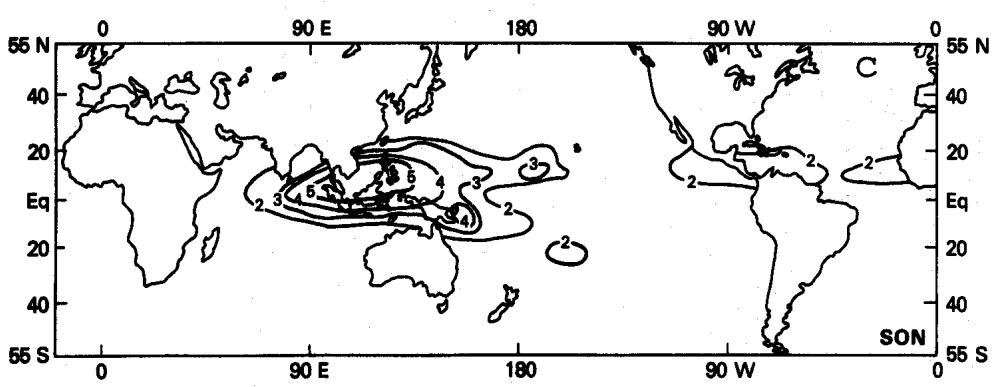

Fig. 9. Seasonal percentage cloud cover caused by optically thin cirrus in the tropics between 25°N and 25°S during September, October, and November. The numbers should be multiplied by 10 to get percent cloud cover.

Next, let us examine the salient aspects of the energetics of the "warm pool". There are two distinct sources of energy that maintain the equilibrium in this local region: (a) the net radiation and (b) the net latent heating. The net radiation input at the top of the atmosphere as measured by ERBE (Barkstrom et al[2]) reveals a maximum over this region which is $\sim 80\ W/m^2$. The net latent heating, which is a result of the heat of condensation in the atmosphere minus the heat of evaporation at the sea surface, is about $250\ W/m^2$. In contrast, the small and large-scale transports of heat in the oceans and atmosphere tend to distribute the available energy

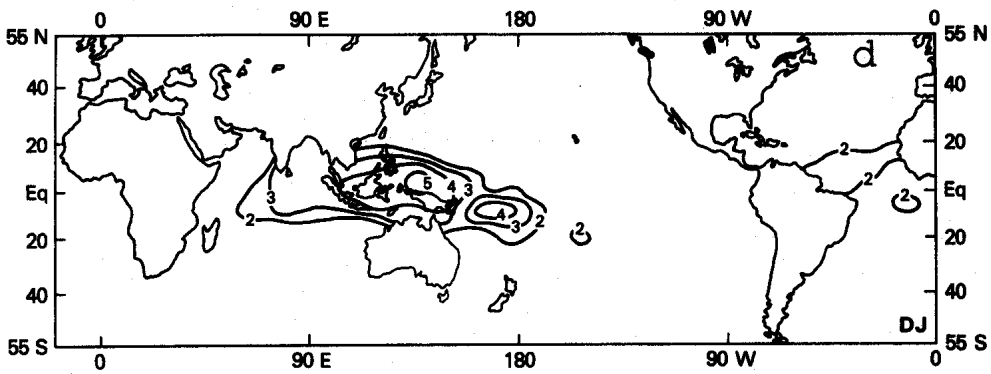

Fig. 10. Seasonal percentage cloud cover caused by optically thin cirrus in the tropics between 25°N and 25°S during December and January. The numbers should be multiplied by 10 to get percent cloud cover.

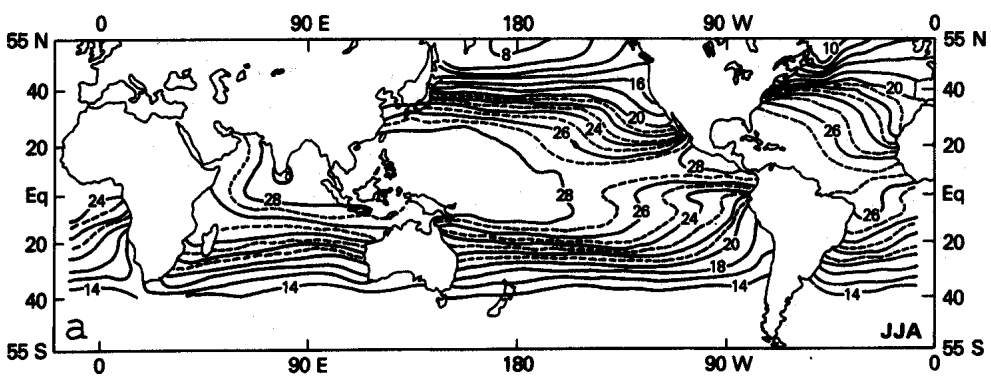

Fig. 11. Climatological sea surface temperature in °C (from Ref. 4) for June, July, and August.

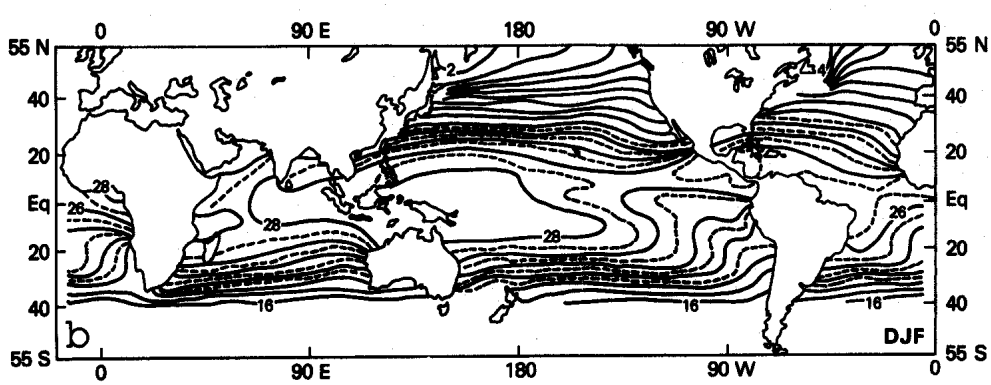

Fig. 12. Climatological sea surface temperature in °C (from Ref. 4) for November, December, and January.

(i.e. net latent heating + net radiative energy) and reduce the temperature maximum in the warm pool.

A schematic diagram of the various processes taking place in the "warm pool" in the presence of MCS is presented in Fig. 1. In the MCS's, some of the cumulonimbus clouds form anvils whose optically thin cirrus covers the sky completely. The lower tropospheric convective cumulus are taken to have cloud tops that reach an average altitude of 5.5 km. If we take the surface temperature to be 301 K and the lapse rate to be 6.5 K/km, then the cumulus cloud tops will have a temperature of 265 K. The cumulus clouds are taken to be blackbodies radiating at the cloud temperature. This means that the cumulus clouds emit 0.6 times the surface flux, σT_s^4, where σ is the Stefan–Boltzmann constant. The cirrus are assumed to be near 12 km and are taken to have a negligible thickness. As before, if we take the surface temperature to be 301 K and the lapse rate to be 6.5 K/km, then the thin cirrus have a temperature of 223 K. This implies that if these thin cirrus were to radiate with an emissivity, ϵ, then their emission would be equal to $0.3\epsilon\sigma T_s^4$. In our formulation, the i.r. emissivity of the cirrus is related to its visible albedo, α, with the help of radiometer measurements obtained from aircraft flights[14] as shown in Table 1. The i.r. transmissivity of the cirrus is given by $(1-\epsilon)$, and its visible transmissivity is $(1-\alpha)$.

A scheme of the radiative energy balance adopted in this study is portrayed in Fig. 13. For our purposes we are considering radiation energy balance in a tropical maritime atmosphere. Spatial and temporal variabilities of the water vapor content and thermal state of the atmosphere as well as the solar input are not crucial in our model. For this reason we can treat the radiation energy balance at the top of the atmosphere in a simple fashion. The important parameters that are varied in our scheme are (1) the cirrus cloud visible albedo which is coupled with the i.r. emissivity and (2) the percentage cumulus cloud cover that is underneath the cirrus. Mainly as a function of the above two cloud parameters the net radiation (i.e. incoming solar minus outgoing i.r.) at the top of the atmosphere are computed.

The upward flux of i.r. radiation emerging at any given pressure level in the atmosphere is calculated using the absorption and emission of the atmospheric gases, water vapor, CO_2 and O_3, as a function of wavenumber using a detailed line-by-line radiation transfer model.[15] The i.r. transmission of the cirrus clouds[16] as a function of wavenumber and columnar ice content (g/cm^2) are computed assuming cirrus ice particles have a mean radius of 6 μm. These spectrally dependent properties of gases and cirrus are then parametrized for use in our simple energy balance model. The cumulus clouds are assumed to have a reflectivity $r = 0.55$.[17]

Table 1. Relationship between the visible albedo and i.r. emissivity of cirrus.

α	ϵ
0.0	0.00
0.1	0.36
0.2	0.63
0.3	0.78
0.4	0.88
0.5	0.94

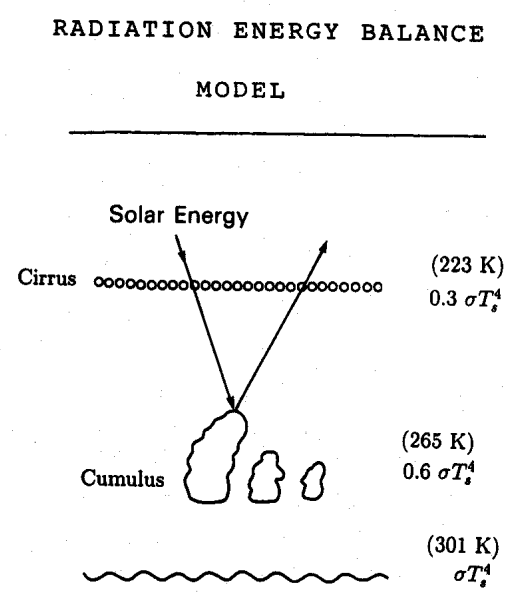

Fig. 13. Schematic diagram showing the radiation energy balance model and its vertical structure.

For an atmosphere having the specified lapse rate and cloud structure we can express the net radiative energy balance, E_{net} between the incoming solar radiation and the outgoing longwave radiation at the top of the atmosphere as:

$$E_{net} = \underbrace{S(1-\alpha)\{[1-\alpha_s(1-\alpha)](1-C)+[1-r(1-\alpha)]C\}}_{\mathrm{I}} - \underbrace{G_1\sigma T_s^4(\epsilon t'+A)}_{\mathrm{II}} - \underbrace{(1-\epsilon)t'[0.6CG_2\sigma T_s^4+(1-C)G_3\sigma T_s^4]}_{\mathrm{III}}, \quad (2)$$

where S is the solar constant, and α_s is the albedo of the cloud free atmosphere and the ocean surface, C is the cumulus cloud fraction, and r is the reflectivity of the cumulus.

The first term on the right-hand side of Eq. (2) is an approximation for the incoming solar energy that is absorbed by the surface–atmosphere system. For present purposes, the diurnal mean insolation near the equator is taken to be $S = 405\ \mathrm{W/m^2}$. Based on satellite measurements, α_s is taken from Gill[18] to be 0.10.

The second term on the right-hand side of Eq. (2) gives the i.r. emission from the cirrus and the overlying atmosphere containing CO_2, O_3, and H_2O. The i.r. flux transmission of the atmospheric absorbing gases above the cirrus level is expressed as $t' = 0.94$. The constant, $A = 0.06$, arises because of the emission of the atmosphere above the cirrus. The constant, G_1, represents the ratio $(T_c/T_s)^4$, which is 0.30 (T_c is the temperature of the cirrus clouds).

The third term on the right-hand side represents the i.r. radiation emerging through the cirrus. This term has two components: (a) a part that corresponds to the emission from the cumulus, and the atmospheric gases between cumulus top and cirrus, and (b) a part that represents the emission from the surface and the atmosphere underlying the cirrus. In here the emission from the cumulus region, that is part (a), is weighted by the cumulus fraction, C, and the other part, (b), is weighted by $(1-C)$. The constants, G_2 and G_3, are scaling constants that are meant to scale the emission from (a) and (b), respectively. This scaling is done to express the emission from these layers in terms of the blackbody radiation from the surface, σT_s^4. The values of G_2 and G_3 are 0.83 and 0.63, respectively. These constants, as well as t' and A, are obtained as stated earlier from spectrally dependent i.r. radiative transfer computations for a tropical atmosphere, assuming $T_s = 301$ K, a lapse rate of 6.5 K/km, 5 g/cm^2 of water vapor, a tropical ozone profile with 0.28 cm of O_3 and a tropopause temperature of 190 K at 17 km.

Eq. (2) may be written in a compact form as:

$$E_{net} = (1-\alpha_c)S - \beta\sigma T_s^4,$$

where

$$\beta = \{G_1(\epsilon t'+A)+(1-\epsilon)t'[0.6CG_2+(1-C)G_3]\} \quad (3)$$

and

$$\alpha_c = \{\alpha_s[(1-C)(1+\alpha^2)+2\alpha C]+(1-2\alpha_s)\alpha + rC(1-\alpha)^2\}.$$

In Eq. (3), α_c is equivalent to an effective albedo and β is the effective emissivity of the Earth–atmosphere system. When $E_{net} = 0$ Eq. (3) may be simplified further as:

$$\sigma T_s^4 = A(1-\alpha_c)/\beta \quad (4)$$

where the ratio $(1-\alpha_c)/\beta$ may be interpreted as a greenhouse amplification factor that takes into account not only the effect of the gases but also the strong interaction of clouds on i.r. and solar radiation.

Based on the formulation given in Eq. (3), β and α_c can be computed as a function of α, the cirrus albedo, with the results being displayed in Fig. 14. In addition in this figure, the dependence of β and α_c on the cumulus cloud cover, C, is distinctly shown. Here the value of r is taken from Stowe et al[17] to be 0.55 and C is given three possible values: 0.1, 0.3, and 0.5. At this point we can calculate the net radiative energy input, E_{net}, from Eq. (3) provided we know T_s.

Varying α_c and β over a range of values and taking the surface temperature to be $T_s = 301$ K, we have estimated E_{net}. These computed values are presented in Fig. 15. We find from this figure

that E_{net} is sensitive to the changes in C and that it decreases by about 10 W/m^2 for 10% increase in cumulus cloud cover C. The maximum net input of energy into the ocean atmosphere system occurs when the cirrus visible albedo is about 0.2, i.e. $\epsilon \approx 0.63$ (see Fig. 14). Based on the approximations developed by Platt and Stephens,[19] we can relate this i.r. emissivity to a total optical depth of approx. 1 for the cirrus cloud. These optimal conditions of energy input are apparently present in the "warm pool" region as evidenced by the IRIS observations (see Figs. 5 and 6), which show that the bulk of the cirrus clouds have optical depths around unity. One may also note from Fig. 15 that the cumulus clouds generally decrease the net energy input to the system.

Following the path of maximum net energy input, which corresponds closely to $\alpha = 0.2$, we find from Fig. 15 that when $C \approx 0.2$, the input energy is about 80 W/m^2. This combination of cirrus and cumulus yields $\alpha_c \approx 0.33$. These estimates of the effective albedo, α_c, and net energy input of $\approx$80 W/m^2 are consistent with the ERBE observations reported by Barkstrom et al[2]. The importance of the thin cirrus clouds can now be elucidated. If the ERBE observed albedo of $\approx$0.33 were the result of only cumulus clouds then the necessary cumulus fraction would be approx. 0.5.

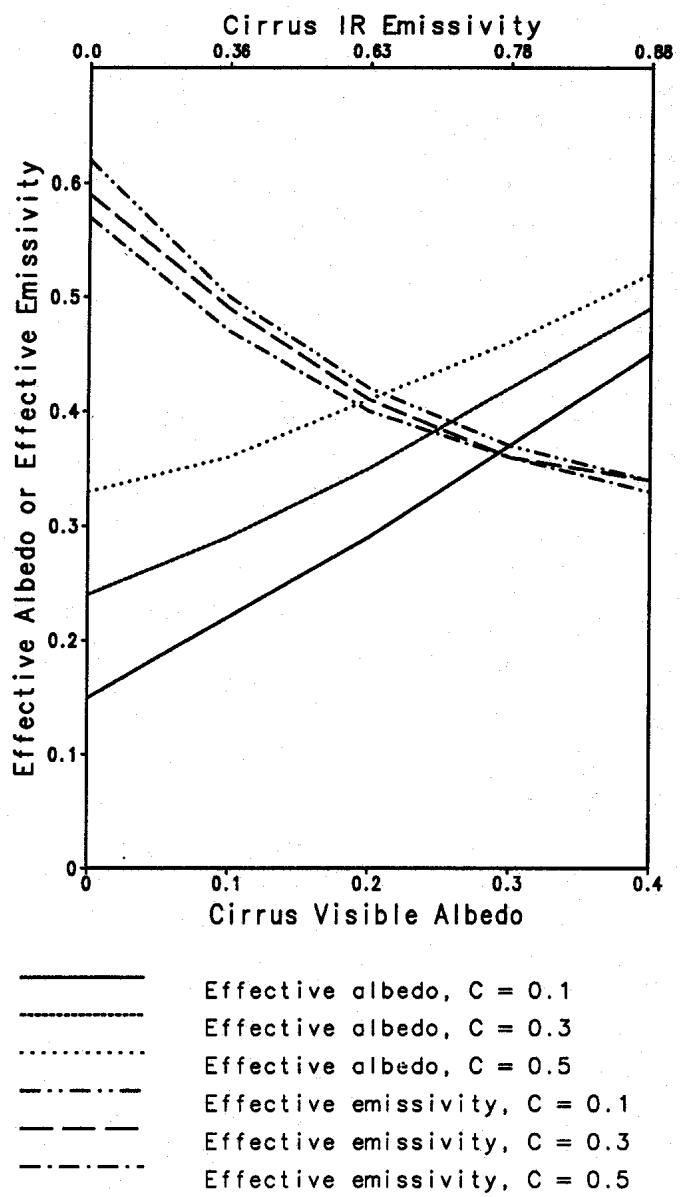

Fig. 14. Dependence of effective albedo, α_c, and effective emissivity, β, on cirrus visible albedo, α. The scale on the ordinate applies to both α_c and β. This dependence is calculated for three different values of the cumulus cloud cover, C. Note the abscissa scale on the top gives the cirrus i.r. emissivity.

According to Fig. 15 this cumulus fraction, with no cirrus over the "warm pool" region, would result in a net radiative energy balance of only $\sim 10\,W/m^2$. This net energy balance is about $70\,W/m^2$ less than that observed by ERBE. Thus, we conclude that the presence of cirrus clouds over the "warm pool" helps conserve a significant amount of the radiative energy and thereby is able to explain the ERBE observations.

To convey the significance of the energy input, we consider as an example a case where only $20\,W/m^2$ of the net radiative energy at the top of the atmosphere is available to heat the ocean water. We find from simple calculations that an ocean mixed layer of 50 m depth will be heated by about 1°C in 100 days.

The radiative energy balance model adopted here may be scrutinized further. In particular, one may examine the parameterization of the cumulus and cirrus cloud temperatures that are scaled in terms of the surface temperature. This parameterization forces the cumulus and cirrus cloud temperature to increase approximately by factors of 0.6 and 0.3, respectively, of the surface temperature increase. Thus, for small perturbations of T_s, taking a constant lapse rate, one can note that the altitude and the pressure level of the clouds remain virtually unchanged. In this coupled

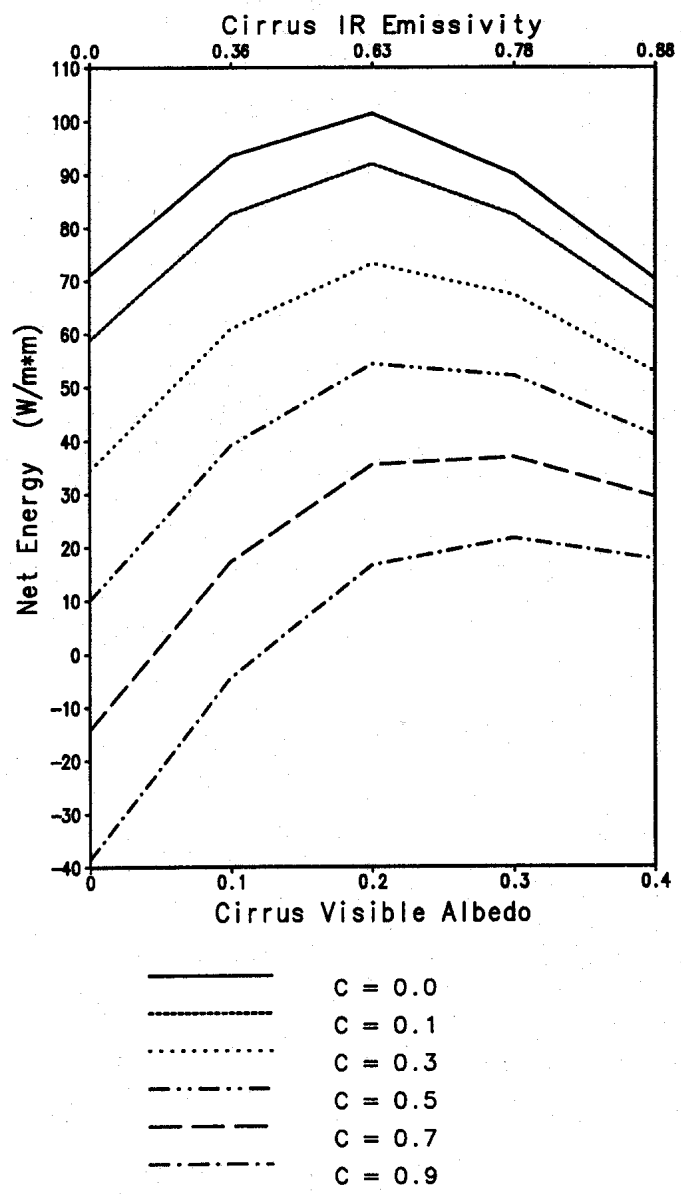

Fig. 15. Dependence of net radiation energy (W/m^2) on cirrus visible albedo for different values of the cumulus cloud cover, C. Note the cirrus i.r. emissivity is given on the top abscissa scale.

cloud temperature system, as the surface temperature increases, i.r. loss to space increases from both the surface and the clouds. This has a moderating effect on T_s variations. If, however, as a counter example, we take the temperature of the cumulus and cirrus clouds to be constant, then the heights of the clouds will increase as T_s increases. Moreover, the i.r. loss to space will depend mainly on T_s, and thus as a consequence, for a given increase in i.r. opacity (such as that caused by an increase in the CO_2 abundance) of the atmosphere and clouds, T_s will increase by a larger amount than that in the scaled cloud temperature case. This is demonstrated in Fig. 16 where the surface temperature variation, as a function of cirrus albedo for both the cases are plotted. The constant cloud temperature scenario leads to a runaway greenhouse effect more quickly than the scaled cloud temperature scenario. The two formulations considered here are anticipated to cover a reasonable range of conditions. Thus, from the results presented here, we expect that the coupled

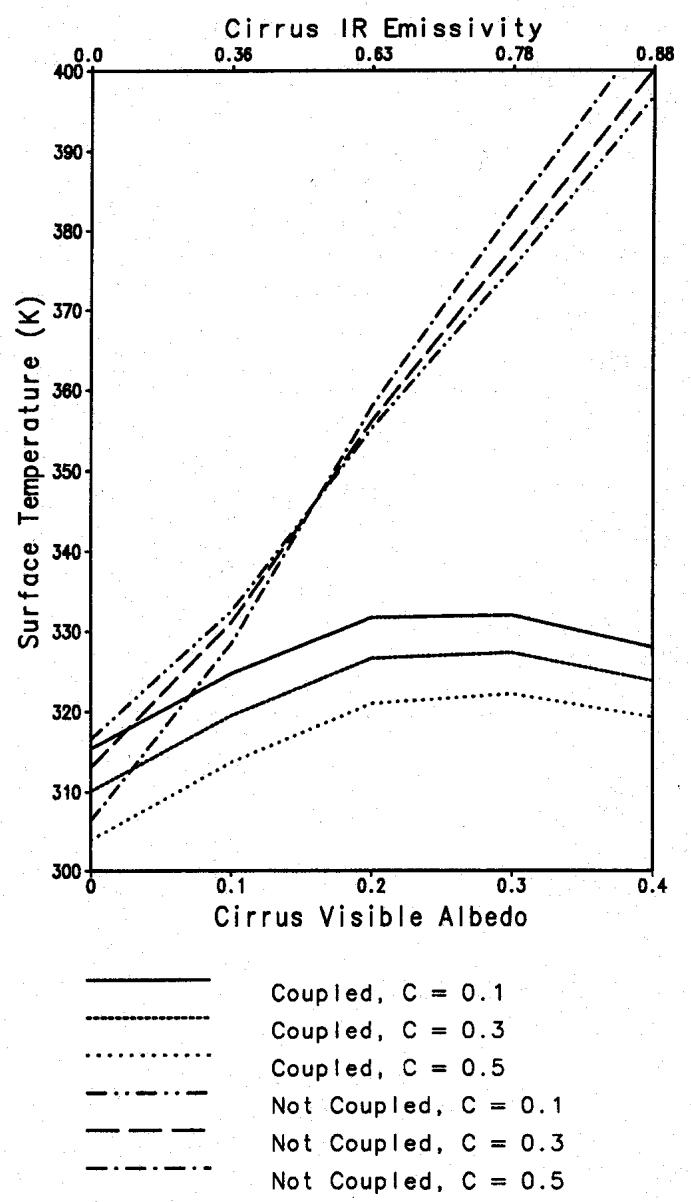

Fig. 16. Dependence of surface temperature (K) on cirrus visible albedo for three different values of the cumulus cloud cover, C. Cirrus i.r. emissivitiy is shown on the top abscissa scale. Surface temperature is computed from Eq. (3) assuming $E_{net} = 0$ for the two hypothetical cases of clouds. In the "coupled" case the temperature of the cumulus and cirrus cloud changes along with that of the surface (this coupling is shown in Fig. 9). In the "uncoupled" case the temperature of the cumulus and cirrus clouds is independent of the surface temperature.

surface and cloud temperature model, which we adopted, will yield conservative estimates of the surface temperature variations.

We conclude from the above analysis that presence of cirrus clouds, that are nearly transparent in the visible and opaque in the i.r. at the cold temperatures high in the upper troposphere leads to a marked greenhouse effect. This conclusion is independent of the radiative energy balance model. This greenhouse warming does not vanish as long as there is a temperature lapse rate $\sim$5–6.5 K/km in the troposphere.

The above analysis of the radiation energy balance is made on the basis of the existence of an MCS and the associated thin cirrus anvil covering an extensive area. When the MCS is absent, as stated earlier, in the "warm pool" region we expect the presence of scattered fair weather cumulus and nearly clear sky conditions. In this situation we again find the net input of radiation (Fig. 15) is about 60–70 W/m^2. Thus, the convective nature of the "warm pool" apparently leads to significant radiation energy input. On the contrary, over the oceanic regions where subsidence and low altitude warm stratiform clouds that reflect visible radiation are dominant, we expect significant cooling. Our energy balance model for the "warm pool" is by no means as exhaustive as the time dependent ocean or atmospheric circulation models which can take into account explicitly all of the processes. All of the relevant input parameters required for such models, however, are not sufficiently well known to draw firm conclusions (see Neelin[20] for a discussion of the air–sea interaction, general circulation models). For this reason we have chosen the simple approach that is described here. The salient inference from this study is that there will be substantially less energy available for the "warm pool" region in the absence of thin cirrus clouds that are optically thin in the visible and not so in the i.r. We believe that with the loss of this energy the "warm pool" may not sustain itself.

During the El Nino events the "warm pool" breaks loose and starts to migrate eastward along the equator. This motion will result in heat loss by mixing with the cool waters of the east. A good example of this migration is the 1982–1983 El Nino event in which the "warm pool" together with its rain pattern moved far into the eastern Pacific in a time span of 10 months. The westerly wind stress[21] which prevailed at that time to the west of the migrating "warm pool" helped the "warm pool" by isolating it. The rainy, cloud-covered migrating "warm pool" system appears to possess all the ingredients of the heating mechanisms that are associated with the stationary event. This means that the migrating "warm pool" is sustained by the sum of the net latent and radiative heatings, which amounts to a total of about 350 W/m^2, in conjunction with the wind stress isolation mechanism.

The importance of the solar control, i.e. the net radiation input, may be appreciated by noting that during the "warm pool's" stationary mode, the "warm pool" mimics the apparent seasonal north–south motion of the sun about the equator. Moreover, there is evidence that even in the migrating mode, the "warm pool" follows the apparent seasonal movement of the sun. This has been inferred from the 1982–1983 event when the centers of the anomalies in OLR and precipitation moved $\sim 5°$ south of the equator in the eastern Pacific.[21] Anomalies in the zonally averaged total water vapor over the eastern Pacific also followed the motion of the subsolar point by moving $\sim 5°$ south in January–February 1983 and then tending to return back to the equator by about June 1983.[22]

The explanation of the heating of the "warm pool" presented in this section relies on a radiative energy balance model which includes observations of thin cirrus clouds. As noted, there are limitations to such a model and thus the conclusions of this section are tentative. At the present time, the coupled ocean–atmosphere models indicate considerable sensitivity to the tropical conditions and suggest that the simulation of "warm pool"/"cold tongue" configuration in the equatorial Pacific represents a challenging test for parameterizations in such models.[20] When these parameterizations are improved one may be able to test our hypothesis of radiative heating of the "warm pool" including the thin cirrus.

4. DISCUSSION AND CONCLUSIONS

Satellite cloud pictures in the visible channel show almost perpetual cloudiness over the western Pacific equatorial regions around Indonesia.[12] If these clouds are of the cumulus or stratiform types

then they have the potential to block a significant amount of solar input energy. Furthermore, it is well known from climatology that the western equatorial Pacific is a region of heavy precipitation as well as an area with warm sea surface temperature. This is also a region of maximum net radiative energy input. The coexistence of these clouds, warm waters, and maximum net radiative energy input requires an explanation. The TOGA–COARE program, in which several components of the energy balance pertaining to the "warm pool" region will be measured, is attempting to explain this. The aim of this study is to show that optically thin cirrus clouds, which emanate from the anvils of convective storms in the "warm pool" and cover the area extensively with sufficient optical depth in the i.r. can account for this local maximum in net radiative energy input into this atmosphere–ocean system. This net input amounting to about 80 W/m^2 can play a significant role in the maintenance of warm waters in the "warm pool".

On a global scale, although the sun is the ultimate source of energy, considerations of energy balance lead to the conclusions that the greenhouse effect produced by gases such as H_2O, CO_2 and O_3 is important in maintaining the relatively warm surface temperatures for the Earth. While the transport processes in the atmosphere and oceans are primarily responsible for reducing the thermal contrast between the tropics and polar regions, they have a relatively minor influence on the global mean temperature. For these reasons, a radiative energy balance model which does not consider the large scale fluid transports may be used to calculate the global mean surface temperature assuming a tropospheric temperature profile that follows a prescribed lapse rate.[23,24]

In a localized region, the fluid transport processes can have a significant influence on heat and moisture. At present coupled ocean–atmosphere models[19] do not explain the maintenance of the "warm pool" satisfactorily. On the other hand, a local maximum in net radiative energy input into the ocean–atmosphere system revealed by ERBE suggests a plausible mechanism for the maintenance of the "warm pool". This study shows that the thin cirrus clouds that are revealed by the satellite data are instrumental in generating this local maximum in radiative energy input. The line of reasoning and the simple physical approach taken here is based on the view: "It is at least possible that the vastly complicated dynamics of the atmosphere and ocean is governed by some overall 'law' which describes the macroscopic behaviour of the system in terms of the external parameters. Since also the significant parameters external to the system are purely radiative energy flows, such a law is likely to be defined in terms of the properties of those flows. The detailed dynamical processes might then be regarded purely as passive variables which adopt values appropriate to satisfying the overall law or boundary condition."[25]

Acknowledgement—One of us (A.V.) acknowledges support by NSF under grant No. ATM-9114318.

REFERENCES

1. O. Garcia, "Atlas of highly reflective clouds for the global tropics: 1971–1983", U.S. Department of Commerce, NOAA Environmental Research Lab., Boulder, CO (1985).
2. B. Barkstrom, E. Harrison, G. Smith, R. Green, J. Kibler, R. Cess, and the ERBE Science Team, *Bull Am. Meteor. Soc.* **70,** 1254 (1989).
3. C. E. Dorman and R. H. Bourke, *Mon. Wea. Rev.* **107,** 896 (1979).
4. World Climate Research Programme, A coupled ocean–atmosphere response experiment for the warm pool regions of the western Pacific. Scientific plan for the TOGA coupled ocean–atmosphere response experiment (COARE), Draft (July 1989).
5. C. M. R. Platt, *Nature* **341,** 428 (1989).
6. V. Ramanathan, R. D. Cess, E. F. Harrison, P. Minnis, B. R. Barkstrom, E. Ahmad, and D. Hartmann, *Science* **243,** 57 (1989).
7. G. L. Stephens, *J. Atmos. Sci.* **37,** 435 (1980).
8. G. L. Stephens and P. J. Webster, *J. Atmos. Sci.* **38,** 235 (1981).
9. R. A. Hanel, B. J. Conrath, V. G. Kunde, C. Prabhakara, I. Revah, V. V. Salomonson, and G. Wolford, *J. Geophys. Res.* **77,** 2629 (1972).
10. C. Prabhakara, R. S. Fraser, G. Dalu, Man-Li C. Wu, and R. J. Curran, *J. Appl. Meteor.* **27,** 379 (1989).
11. T. Inoue. *J. Met. Soc. Jap.* **63,** 88 (1985).
12. L. L. Stowe, H. Y. M. Yeh, T. F. Eck, C. G. Wellemeyer, H. L. Kyle, and the Nimbus-7 Cloud Data Processing Team, *J. Clim.* **2,** 671 (1989).
13. C. M. R. Platt, J. C. Scott, and A. C. Dilley, *J. Atmos. Sci.* **44,** 729 (1987).
14. J. D. Spinhirne and W. D. Hart, *Mon. Wea. Rev.* **118,** 2329 (1990).
15. D. P. Kratz, B.-C. Gao, and J. T. Kiehl, *JGR* **96,** 9021 (1991).

16. C. Prabhakara, J.-M. Yoo, G. Dalu, and R. S. Fraser, *JAM* **29,** 1313 (1990).
17. L. L. Stowe, C. G. Wellemeyer, T. F. Eck, H. Y. M. Yeh, and the Nimbus-7 Cloud Data Processing Team, *J. Clim.* **1,** 445 (1988).
18. A. E. Gill, *Atmosphere–Ocean Dynamics*, Academic Press, New York, NY (1982).
19. C. M. R. Platt and G. L. Stephens, *J. Atmos. Sci.* **37,** 2314 (1980).
20. J. D. Neelin, M. Latif, M. A. F. Allaart, M. A. Cane, U. Cubash, W. L. Gates, P. R. Gent, M. Ghil, C. Gordon, N. C. Lau, C. R. Mechoso, G. A. Meehl, J. M. Oberhuber, S. G. H. Philander, P. S. Schopf, K. R. Sperber, A. Sterl, T. Tokioka, J. Tribbia, and S. E. Zebiak, *Clim. Dynamics* **7,** 73 (1992).
21. E. M. Rasumsson and J. M. Wallace, *Science* **222,** 1195 (1983).
22. C. Prabhakara, D. A. Short, and B. E. Vollmar, *J. Clim. Appl. Meteor.* **24,** 1311 (1985).
23. A. Arking, *Bull. Am. Meteor. Soc.*, in press (1993).
24. V. Ramanathan and J. A. Coakley, Jr, *Rev. Geophys. Space Phys.* **16,** 465 (1978).
25. G. W. Paltridge and G. M. Platt, *Radiative Transfer Processes in Meterology and Climatology*, p. 32, Elsevier, New York, NY (1976).